J|A|C|S
ARTICLES

Published on Web 04/14/2010

Do [*all*]-*S*,*S*′-Dioxide Oligothiophenes Show Electronic and Optical Properties of Oligoenes and/or of Oligothiophenes?

María Moreno Oliva,[†] Juan Casado,*[,†] Juan T. López Navarrete,*[,†] Serguei Patchkovskii,[‡] Theodore Goodson III,[⊥] Michael R. Harpham,[⊥] J. Sérgio Seixas de Melo,[¶] Elizabeta Amir,[□] and Shlomo Rozen[□]

Department of Physical Chemistry, University of Málaga, Campus de Teatinos s/n, Málaga 29071, Spain, Steacie Institute for Molecular Sciences, National Research Council of Canada, 100 Sussex Drive, Ottawa, K1A 0R6 Canada, Department of Chemistry, University of Michigan, Ann Arbor, Michigan 48109, Department of Chemistry, University of Coimbra, 3004-535 Coimbra, Portugal, and School of Chemistry, Raymond and Beverly Sackler Faculty of Exact Sciences, Tel Aviv University, Tel Aviv 69978, Israel

Received February 4, 2010; E-mail: casado@uma.es; teodomiro@uma.es

Abstract: A comprehensive photophysical and spectroscopic (electronic and Raman) study guided by density functional theory, DFT, CIS, and correlated ab initio calculations has been performed on a series of fully oxidized oligothiophenes with variable chain length, and up to four rings. A comparison with the properties of oligoenes and oligothiophenes is proposed. Absorption, fluorescence, lifetimes, flash-photolysis, phosphorescence, two-photon absorption, Raman, resonance Raman, and thermospectroscopy data are collected and interpreted according to the obtained theoretical results. The interest is focused on the ground electronic state and in the low-lying excited electronic states. Full oxygenation of the sulfur atoms of oligothiophenes results in: (i) restricted inter-ring isomerization such as observed from the absorption spectra; (ii) an effective quenching of fluorescence, and (iii) the appearance of dual emission. The emission features are explained by the interference of a dipole-allowed and a dipole-forbidden singlet excited states leading to simultaneous lighting from a local Frenkel and an intramolecular charge transfer photon-releasing configurations. These two excited states contribute to the broadening of the light emission spectrum. These properties highlight the similarity of these samples to that of oligoenes with comparable number of π-electrons.

1. Introduction

There exists a great interest in oligothiophene (OTh) chemistry[1] since the applications of these molecules as electro-, photo-, and NLO-active substrates in organic devices such as field-effect transistors (OFET),[1,2] light-emitting diodes (OLED) and photovoltaics,[1,3,4] biological applications,[4] lasers,[4,5] etc. Since Garnier's pioneering work with sexithiophene,[6] where this compound was successfully implemented in an OFET device, many other derivatives have been presented with a variety of notable improvements.[1,2] Among these, the sulfone or *S*,*S*′-dioxide derivatives, where the thienyl sulfur is oxidized to its dioxide state, have been exploited pursuing two complementary properties: (i) the gaining of electron affinity for better electrochemical reduction and n-channel behavior in OFETs (note that sulfur oxidation has been also used to tune p- or hole-mobility to n- or electron-conduction),[4,7] and (ii) the "surprising" increment of photoluminescence efficiency in solid state relative to its solution behavior (i.e., usually the photoluminescence quantum yield is lower in solution) which is critical for improved OLEDs and optically pumped lasers.[4,5] However, it must be stressed that most of these studies on the dioxide samples have dealt with partially oxidized oligothiophenes mainly due to the synthetic difficulties in obtaining the fully oxidized compounds.[4,5] This fact has, to some extent, precluded a more in-depth knowledge of the electronic, structural, and photophysical improvements than the strategy of sulfonation of thiophene oligomers may offer.

Interest in polythiophenes and oligothiophenes was fueled by the realization of the low photochemical stability and poor thermal resistance of polyacetylene and their oligomers (written as oligoenes or OEO hereafter) which limited the development of applications based on them.[8] In this regard, oligophenylene derivatives (OPh) have been also intensively studied as chemically resistant samples, but the strong aromaticity of the benzene group has a limiting effect in a series of properties.[9] As a compromise between these two (i.e., oligoenes and oligophenylene derivatives), oligothiophenes[1,2,4] offer much greater

[†] University of Málaga.
[‡] Steacie Institute for Molecular Sciences, National Research Council of Canada.
[⊥] University of Michigan.
[¶] University of Coimbra.
[□] Raymond and Beverly Sackler Faculty of Exact Sciences, Tel Aviv University.

(1) (a) Mishra, A.; Ma, C.-Q.; Baüerle, P., *Chem. Rev* **2009**, *109*, 1141. Roncali, J. *Chem. Rev.* **1997**, *97*, 173. (b) Fichou, D. *J. Mater. Chem.* **2000**, *10*, 571–588. (c) Shirota, Y. *J. Mater. Chem.* **2000**, *10*, 1. (d) Mitschke, U.; Baüerle, P. *J. Mater. Chem.* **2000**, *10*, 1471. (e) Perepichka, I. F., Perepichka, D. F., Eds. *Handbook of Thiophene-Based Materials: Applications in Organic Electronics and Photonics*; Wiley: New York, 2009.

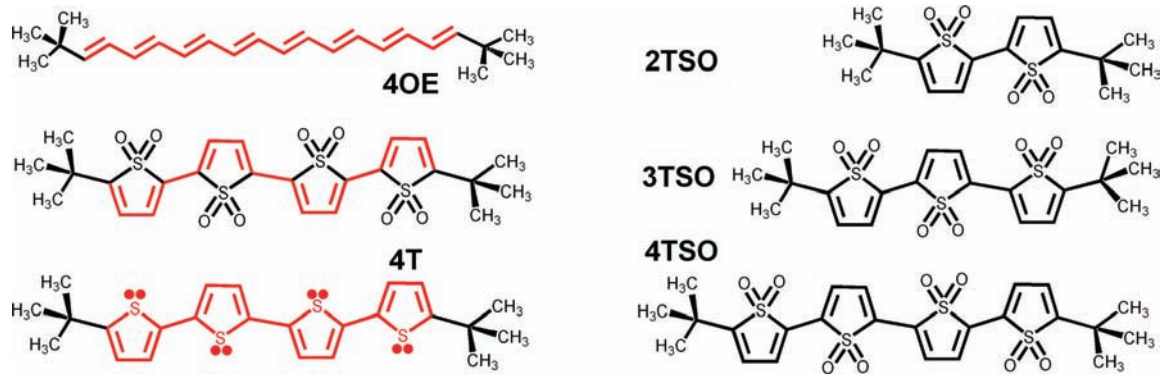

Figure 1. Chemical structures and acronyms of the compounds studied. The π-conjugated paths are shown in red.

chemical and thermal stability than polyenes having a moderate ring aromaticity (much lower than in OPh) which leads to a large inter-ring π-electron delocalization and conjugated molecules with low or very low band gap, interesting luminescence features, and excellent redox activity.

Recently, some of us (E.A. and S.R.) utilized HOF·CH_3CN, the best oxygen transfer agent available that possesses a truly electrophilic oxygen moiety,[10] for transferring oxygen atoms to all sulfurs of oligothiophenes.[11] This gives us a unique opportunity to study the electronic and structural properties of these fully oxidized oligothiophenes and to further complete the previous knowledge on the partially oxidized compounds mainly coming from the group of Barbarella.[4] Our hypothesis states that oxidation of the sulfur atom of oligothiophenes decouples the pair of electrons of S from the thiophene ring aromaticity ($4n + 2$ rule), leading these oligomers to gain oligoene character. The evaluation of a set of molecular properties to try to get insights into the evolution of the *S*,*S*′-dioxide oligothienyl properties in Figure 1 from oligothiophene to oligoenes is the focus of this work with an overall goal of analyzing optical and electronic features likely exploitable in organic electronics.

The present work is composed of photophysical data (i.e., absorption, luminescence, lifetimes, flash-photolysis, phosphorescence, and two-photon absorption) and Raman spectroscopic results (i.e., resonance and nonresonance Raman and thermospectroscopy) and accounts for them with the help of theoretical data in the framework of the DFT and CIS methods together with correlated multireference (MRQDPT2) calculations needed to account for excited-states properties, especially those with multiconfigurational character. In section 2.1, the optical properties and photophysical data are presented and discussed in terms of the competition of the relevant electronic excited states. In section 2.2, the Raman spectra are used to address their conjugational properties, and to provide new vibrational signatures of the electronic excited states presented in the previous section. In the Results and Discussion, the properties of the new oligomers are discussed as compared to those of the oligoenes and oligothiophenes. Some conclusions useful for the design and future work on the dioxide oligothiophenes in organic electronics are presented in the final section of the paper.

2. Results and Discussion

2.1. Absorption Spectra and Electronic Structure. 2.1.1. Energy Behavior and Orbital Composition. The absorption spectra of the dioxide oligothiophenes and the spectrum of **4TSO** are compared in Figure 2 with that of the nonoxidized tetramer (i.e., **4T**) and of the *all-trans*-di(terbutyl)-16-octaene[12] (i.e., **4OE**) which is the **4TSO** oligoene homologue with eight alternating double bonds.

(2) (a) Garnier, F.; Hajlaoui, R.; Yassar, A.; Srivastava, P. *Science* **1994**, *265*, 1684. (b) Li, X.-C.; Sirringhaus, H.; Garnier, F.; Holmes, A. B.; Moratti, S. C.; Feeder, N.; Clegg, W.; Teat, S. J.; Friend, R. H. *J. Am. Chem. Soc.* **1998**, *120*, 2206. (c) Laquindaum, J. G.; Katz, H. E.; Lovinger, A. J. *J. Am. Chem. Soc.* **1998**, *120*, 664. (d) Ponomarenko, S.; Kirchmeyer, S.; Elschner, A.; Huisman, B. H.; Karbach, A.; Dreschler, D. *Adv. Funct. Mater.* **2003**, *13*, 591. (e) Mushrush, M.; Facchetti, A.; Lefenfeld, M.; Katz, H. E.; Marks, T. J. *J. Am. Chem. Soc.* **2003**, *125*, 9414. (f) Newman, C. R.; Frisbie, C. D.; da Silva Filho, D. A.; Brédas, J. L.; Ewbank, P. C.; Mann, K. R. *Chem. Mater.* **2004**, *16*, 4436. (g) Pappenfus, T. M.; Chesterfield, R. J.; Frisbie, C. D.; Mann, K. R.; Casado, J.; Raff, J. D.; Miller, L. L. *J. Am. Chem. Soc.* **2002**, *124*, 4184. (h) Chesterfield, R. J.; Newman, C. R.; Pappenfus, T. M.; Ewbank, P. C.; Haukaas, M. H.; Mann, K. R.; Miller, L. L.; Frisbie, C. D. *Adv. Mater.* **2003**, *15*, 1278. (i) Dimitrakopoulos, C. D.; Malenfant, P. R. L. *Adv. Mater.* **2002**, *14*, 99. (j) Otsubo, T.; Aso, Y.; Takimiya, K. *J. Mater. Chem.* **2002**, *12*, 2565.

(3) (a) Roncali, J. *Chem. Soc. Rev.* **2005**, *34*, 483. (b) Lu, J.; Xia, P. F.; Lo, P. K.; Tao, Y.; Wong, M. S. *Chem. Mater.* **2006**, *18*, 6194. (c) Li, Z. H.; Wong, M. S.; Tao, Y.; Fukutani, H. *Org. Lett.* **2007**, *9*, 3659. (d) Perepichka, I. F.; Perepichka, D. F.; Meng, H.; Wudl, F. *Adv. Mater.* **2005**, *17*, 2281. (e) Suzuki, M.; Fukuyama, M.; Hori, Y.; Hotta, S. *J. Appl. Phys.* **2002**, *91*, 5706. (f) Hiramatsu, T.; Shimada, T.; Hotta, S.; Yanagi, H. *Thin Solid Films* **2008**, *516*, 2700.

(4) (a) Barbarella, G.; Favaretto, L.; Sotgiu, G.; Zambianchi, M.; Antolini, L.; Pudova, O.; Bongini, A. *J. Org. Chem.* **1998**, *63*, 5497. (b) Barbarella, G.; Favaretto, L.; Sotgiu, G.; Zambianchi, M.; Arbizzani, C; Bongini, A.; Mastragostino, M. *Chem. Mater.* **1999**, *11*, 2533. (c) Barbarella, G.; Favaretto, L.; Sotgiu, G.; Zambianchi, M.; Fattori, V.; Cocchi, M.; Cacialli, F.; Gigli, G.; Cingolani, R. *Adv. Mater.* **1999**, *11*, 1375. (d) Barbarella, G.; Favaretto, L.; Sotgiu, G.; Zambianchi, M.; Bongini, A.; Arbizzani, C.; Mastragostino, M.; Anni, M.; Gigli, G.; Cingolani, R. *J. Am. Chem. Soc.* **2000**, *122*, 11971. (e) Gigli, G.; Inganas, O.; Anni, M.; De Vittorio, M.; Cingolani, R.; Barbarella, G.; Favaretto, L. *Appl. Phys. Lett.* **2001**, *78*, 1493. (f) Pisignano, D.; Anni, M.; Gigli, G.; Cingolani, R.; Zavelani-Rossi, M.; Lanzani, G.; Barbarella, G.; Favaretto, L. *Appl. Phys. Lett.* **2002**, *81*, 3534. (g) Pasini, M.; Destri, S.; Porzio, W.; Botta, C.; Giovanella, U. *J. Mater. Chem.* **2003**, *13*, 807. (h) Barbarella, G.; Melucci, M.; Sotgiu, G. *Adv. Mater.* **2005**, *17*, 1581. (i) Ridolfi, G.; Camaioni, N.; Samori, P.; Gazzano, M.; Accorsi, G.; Armaroli, N.; Favaretto, L.; Barbarella, G. *J. Mater. Chem.* **2005**, *15*, 895. (j) Mariano, F.; Mazzeo, M.; Duan, Y.; Barbarella, G.; Favaretto, L.; Carallo, S.; Cingolani, R.; Gigli, G. *Appl. Phys. Lett.* **2009**, *94*, 063510. (k) Melucci, M.; Frere, P.; Allain, M.; Levillain, E.; Barbarella, G.; Roncali, J. *Tetrahedron* **2007**, *63*, 9774. (l) Lattante, S.; Barbarella, G.; Favaretto, L.; Gigli, G.; Cingolani, R.; Anni, M. *Appl.Phys. Lett.* **2006**, *89*, 051111/1.

(5) (a) Garnier, F.; Horowitz, G.; Valat, P.; Fayçal, K.; Wintgens, V. *Appl. Phys.Lett.* **1998**, *72*, 2087. (b) Samuel, I. D. W.; Turnbull, G. A. *Chem. Rev.* **2007**, *107*, 1272. (c) Yamao, T.; Yamamoto, K.; Taniguchi, Y.; Hotta, S. *Appl.Phys. Lett.* **2007**, *91*, 201117/1. (d) Bando, K.; Nakamura, T.; Masumoto, Y.; Sasaki, F.; Kobayashi, S.; Hotta, S. *J. Appl. Phys.* **2006**, *99*, 013518/1. (e) Ichikawa, M.; Hibino, R.; Inoue, M.; Haritani, T.; Hotta, S.; Koyama, T.; Taniguchi, Y. *Adv. Mater.* **2003**, *15*, 213.

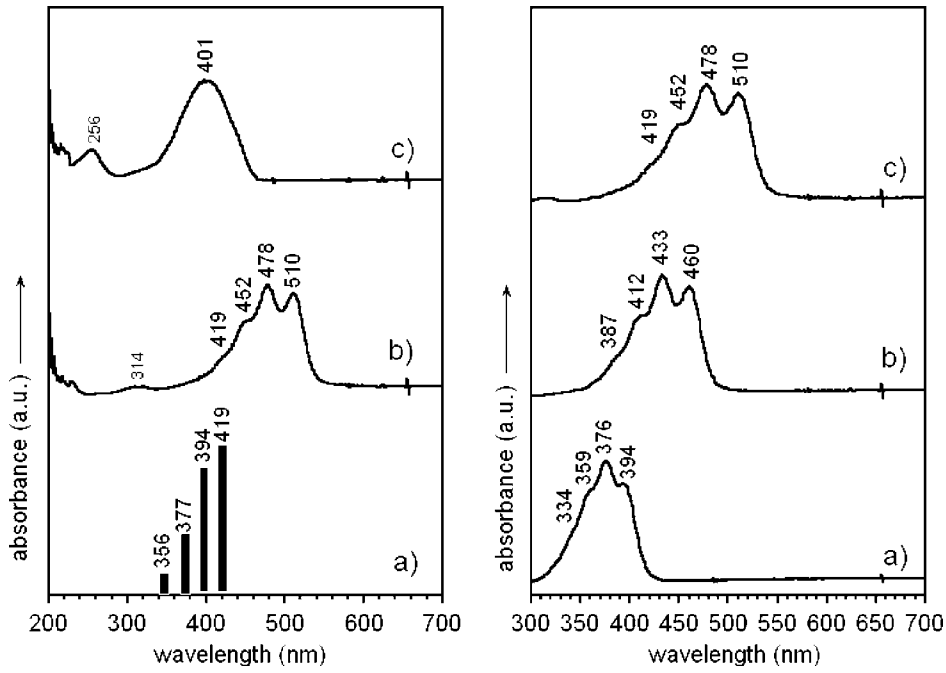

Figure 2. Left: UV−vis absorption spectra in dichloromethane of (a) **4OE** represented as bars keeping the experimental relative intensities as in ref 12; (b) **4TSO**, and (c) **4T**. Right: (a) **2TSO**, (b) **3TSO**, and (c) **4TSO**.

A substantial 77 nm red-shift of the absorption maximum and the emergence of well-resolved vibronic peaks are produced by full oxidation of the sulfur atoms of **4T** to **4TSO**. On the other hand, the electronic absorption of **4OE** is blue-shifted by approximately 90 nm relative to **4TSO**. DFT calculations in Figure S1 (Supporting Information) and in Table 1 can be used to understand this behavior. In particular, adiabatic excited-state calculations, with the time-dependent protocol in DFT (TD-DFT//B3LYP/6-31G**), allow the assignment of the main experimental absorption at 401 nm (3.09 eV) in **4T** to the first $S_0 \rightarrow S_1$ excitation ($1^1A_g \rightarrow 1^1B_u$; HOMO→LUMO) calculated at 2.76 eV; similarly in **4TSO**, the measured absorption band is at 478−510 nm (2.59−2.43 eV) and can be assigned to the $S_0 \rightarrow S_1$ excitation ($1^1A_g \rightarrow 1^1B_u$; HOMO→LUMO) predicted at 2.16 eV, thus reproducing the experimental red-shift from **4T** to **4TSO**. For **4OE** the low-lying band in the absorption spectrum, recorded at 394−419 nm (3.15−2.96 eV), was theoretically predicted at 2.62 eV, falling between the absorptions of **4T** and **4TSO**. These excitations are found to be mainly due to the HOMO-to-LUMO single excitations (see Figure S1 in Supporting Information for orbital topologies).

Table 1. TD-DFT//B3LYP/6-31G** Energies, Oscillator Strengths (*f*) and Description of the Two Low-Lying Theoretical Singlet Excitations of **4T**, **4TSO**, and **4OE**

	4T	4TSO	4OE
$1^1A_g \rightarrow 1^1B_u$	2.76 (449), $f = 1.48$	2.16 (571), $f = 1.31$	2.63 (472), $f = 3.52$
orbital comp.	H→L	H→L	H→L
$1^1A_g \rightarrow 2^1A_g$	3.45 (359), $f = 0$	2.70 (459), $f = 0$	3.09 (402), $f = 0$
orbital comp.	H−1→L + H→L+1	H−1→L + H→L+1	H−1→L + H→L+1

Both the HOMO and LUMO are stabilized upon oxidation; however, the LUMO is affected more strongly than the HOMO (1.91 eV vs 1.09 eV for **2T→2TSO**), causing a shift of the electronic absorption to lower energy. The molecular consequences of oxidation is the removal of the 2 p_z electrons of each sulfur atom from thiophene ring aromaticity, transforming π-electron density into new α-bonds, overall resulting in a lowering of the number of π-orbitals and in their displacement to lower energies (see Figure S1, Supporting Information).

In **2OE**, the HOMO is higher in energy than in **2TSO** due to the better electron conjugation in an *all-trans* C═C/C−C

(6) Horowitz, G.; Fichou, D.; Peng, X.; Xu, Z.; Garnier, F. *Solid State Commun.* **1989**, *72*, 381. Fichou, D.; Horowitz, G.; Nishikitani, Y.; Garnier, F. *Chemtronics* **1988**, *3*, 176.
(7) (a) Casado, J.; Zgierski, M. Z.; Ewbank, P. C.; Burand, M. W.; Janzen, D. E.; Mann, K. R.; Pappenfus, T. M.; Berlin, A.; Perez-Inestrosa, E.; Ortiz, R. P.; Lopez Navarrete, J. T. *J. Am. Chem. Soc.* **2006**, *128*, 10134. (b) Pappenfus, T. M.; Melby, J. H.; Hansen, B. B.; Sumption, D. M.; Hubers, S. A.; Janzen, D. A.; Ewbank, P. C.; McGee, K. A.; Burand, M. W.; Mann, K. R. *Org. Lett.* **2007**, *9*, 3721. (c) Suzuki, Y.; Okamoto, T.; Wakamiya, A.; Yamaguchi, S. *Org. Lett.* **2008**, *10*, 3393. (d) Suh, M. C.; Jiang, B.; Tilley, T. D. *Angew. Chem., Int. Ed.* **2000**, *39*, 2870.
(8) (a) Lawrentz, U.; Grahn, W.; Lukaszuk, K.; Klein, C.; Wortmann, R.; Feldner, A.; Scherer, D. *Chem.—Eur. J.* **2002**, *8*, 1573. (b) Elandaloussi, E. D.; Frére, P.; Richomme, P.; Orduna, J.; Garín, J.; Roncali, J. *J. Am. Chem. Soc.* **1997**, *119*, 10774. Roncali, J. *Acc. Chem. Res.* **2000**, *33*, 147. (c) Kohler, B. E. *Chem. Rev.* **1993**, *93*, 41. (d) Mishra, A.; Behera, R. K.; Behera, P. K.; Mishra, B. K. *Chem. Rev.* **2000**, *100*, 1973.
(9) (a) McGehee, M. D.; Heeger, A. J. *Adv. Mater.* **2000**, *12*, 1655. (b) Jonkheijm, P.; Stutzmann, N.; Chen, Z.; de Leeuw, D. M.; Meijer, E. W.; Schenning, A. P. H. J.; Wuerthner, F. *J. Am. Chem. Soc.* **2006**, *128*, 9535. (c) van Herrikhuyzen, J.; Janssen, R. A. J.; Meijer, E. W.; Meskers, S. C. J.; Schenning, A. P. H. J. *J. Am. Chem. Soc.* **2006**, *128*, 686. (d) Simpson, C. D.; Mattersteig, G.; Martin, K; Gherghel, L.; Bauer, R. E.; Raeder, H. J.; Muellen, K *J. Am. Chem. Soc.* **2004**, *126*, 3139. (e) Neuteboom, E. E.; Meskers, S. C. J.; Van Hal, P. A.; Van Duren, J. K. J.; Meijer, E. W.; Janssen, R. A. J.; Dupin, H.; Pourtois, G.; Cornil, J.; Lazzaroni, R.; Bredas, J.-L.; Beljonne, D. *J. Am. Chem. Soc.* **2003**, *125*, 8625. (f) Schenk, R.; Gregorius, H.; Meerholz, K.; Heinze, J.; Muellen, K. *J. Am. Chem. Soc.* **1991**, *113*, 2634. (g) Robinson, M. R.; Wang, S.; Bazan, G. C.; Cao, Y. *Adv. Mater.* **2000**, *12*, 1701. (h) Wang, S.; Bazan, G. C.; Tretiak, S.; Mukamel, S. *J. Am. Chem. Soc.* **2000**, *122*, 1289. (i) Friend, R. H.; Gymer, R. W.; Holemes, A. B.; Burroughes, J. M.; Marks, R. N.; Taliani, C.; Bradley, D. D. C.; Dos Santos, D. A.; Brédas, J. L.; Logdlund, M.; Salaneck, W. R. *Nature* **1999**, *397*, 121.
(10) (a) Rozen, S.; Brand, M. *Angew. Chem., Int. Ed.* **1986**, *25*, 554. (b) Rozen, *Eur. J. Org. Chem.* **2005**, 2433.
(11) Amir, E.; Rozen, S. *Angew. Chem., Int. Ed.* **2005**, *44*, 7374.
(12) (a) Chance, R. R.; Schaffer, H.; Knoll, K.; Schrock, R.; Silbey, R. *Synth. Met.* **1992**, *49*−*50*, 271. (b) Knoll, K.; Schrock, R. *J. Am. Chem. Soc.* **1989**, *111*, 7989.

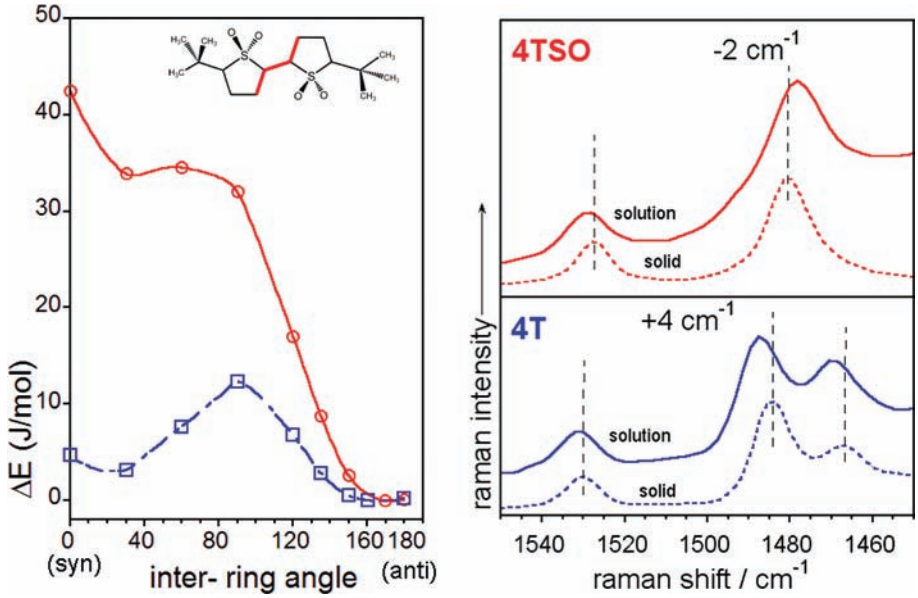

Figure 3. Left: dihedral energy profile with ΔE as the energy difference regarding the optimized structure. Blue line: **4T** and red line: **4TSO**. The inset shows in red the dihedral angle between the two rings. Right: Raman spectra in solution and in solid state.

skeleton. In contrast to **4OE**, the antibonding interactions in the LUMO wave function are caused by the carbon−sulfur bonds of **4T**, accounting for the higher energy in the sulfur derivative. Upon oxidation, the sulfur in **4TSO** is found to become nonbonding. Also in this empty orbital some electron density is displayed by the oxygen atoms which, given their high electronegativity, produce the marked LUMO stabilization relative to **4T** and **4OE**. These electronic effects also have a strong influence in their redox properties relative to nonoxidized oligothiophenes: (i) the appearance of reductions is due to the LUMO stabilization, and (ii) the destabilization of the oxidations is a consequence of the energy lowering of the HOMO.[10]

2.1.2. Spectral Shape and Molecular Conformers. A broad and featureless electronic absorption band resulting from the envelope of the bands of the various conformers (conformational flexibility), present or populated at room temperature in the ground state,[13] is shown by nonoxidized oligothiophenes (e.g., our disubstituted terbutyl ones). However, clear vibronic activity with four well-differentiated peaks for the intense low-lying absorption is shown by **4OE**. In this sense the oligoene property with the similar four-peak structure for the $S_0 \rightarrow S_1$ electronic band is retained by the dioxide oligothiophenes.

Commonly, it is recurred to the consideration of planarity or rigidity of the molecular backbone in the ground electronic state to address the appearance of vibronic peaks.[13] In the next sections (Figures 4 and 11) the optimized geometries of the S_0 and S_1 states are considered for **3T** and **3TSO** and **4TSO** as representative examples. The DFT ground electronic state of **3T** is slightly less distorted from planarity than that of **3TSO** (i.e., by 4.7° for the C═C−C═C dihedral angle); however, the central inter-ring C−C distance is shorter in **3TSO** (i.e., 1.422 Å) than in **3T** (i.e., 1.446 Å). Consequently, **3TSO** is slightly more rigid and less planar than **3T**. To further develop this explanation, the dependence of the formation energy on the dihedral angle between the two rings is shown in Figure 3 for **2TSO** and **2T**, with these two molecules chosen to lower the computational cost of the calculation and reduce the system to having a single dihedral angle.

From Figure 3 it is observed that for **2T** two conformers, manifested by two minima in the S_0 ground electronic state potential energy curve, are accessible within the thermal energy at room temperature (i.e., RT); however, for **2TSO** the situation is found to be rather different as just one isomer is observed to be stable by distortion around this angle, leading to the contribution of a single conformer and the appearance of vibronic subpeaks. The vibronic features of **4OE** are similarly explained; a unique *all-trans* conformer is likely caused by the presence of a high energy barrier to isomerization around the quasi-single C−C bonds.

In order to experimentally scan the presence of the mentioned conformers, the solution- and solid-state Raman spectra for **4TSO** and **4T** are displayed in Figure 3. It is observed that for the latter, the strongest conjugational peak (see Raman section) up-shifts by 4 cm^{-1} which is explained by the contribution of more than one conformer in solution (i.e., distortion implies less π-electron conjugation or strengthening of the C═C bonds with a subsequent increment of their stretching frequencies). However, for **4TSO**, the Raman band is shifted to lower energies by 2 cm^{-1}, which is attributed to the presence of a planar conformer. This is a well-known property of partially sulfonated oligothiophenes, in which a distorted conjugational backbone in the solid state simultaneously accounts for their better emission properties (i.e., higher photoluminescence efficiency) in the solid than in solution.[4,7]

In π-conjugated oligomers, vibronic features also arise because of the structural and vibrational similarities between the S_0 and S_1 states.[24] Recently, Millán-Medina[13d] et al. have justified that the vibronic resolution of **EDO4T** (i.e., ethylene-dioxytetrathiophene) is better substantiated by a similarity among the out-of-plane torsional modes of the electronic ground

(13) (a) Cornil, J.; Blejonne, D.; Shuai, Z.; Hagler, T. W.; Campbell, I.; Bradley, D. D. C.; Brédas, J. L.; Spangler, C. W.; Müllen, K. *Chem. Phys. Lett.* **1995**, *247*, 425. (b) Zgierski, M. Z.; Zerbetto, F. *J. Chem. Phys.* **1993**, *99*, 3721. (c) Negri, F.; Zgierski, M. Z. *J. Chem. Phys.* **1994**, *100*, 2571. (d) Millan Medina, B.; Wasserberg, D.; Meskers, S. C. J.; Mena-Osteritz, E.; Bauerle, P.; Gierschner, J. *J. Phys. Chem. A* **2008**, *112*, 13282. (e) Wasserberg, D.; Meskers, S. C. J.; Janssen, R. A.; Mena-Osteritz, E.; Bauerle, P. *J. Am. Chem. Soc.* **2006**, *128*, 17007.

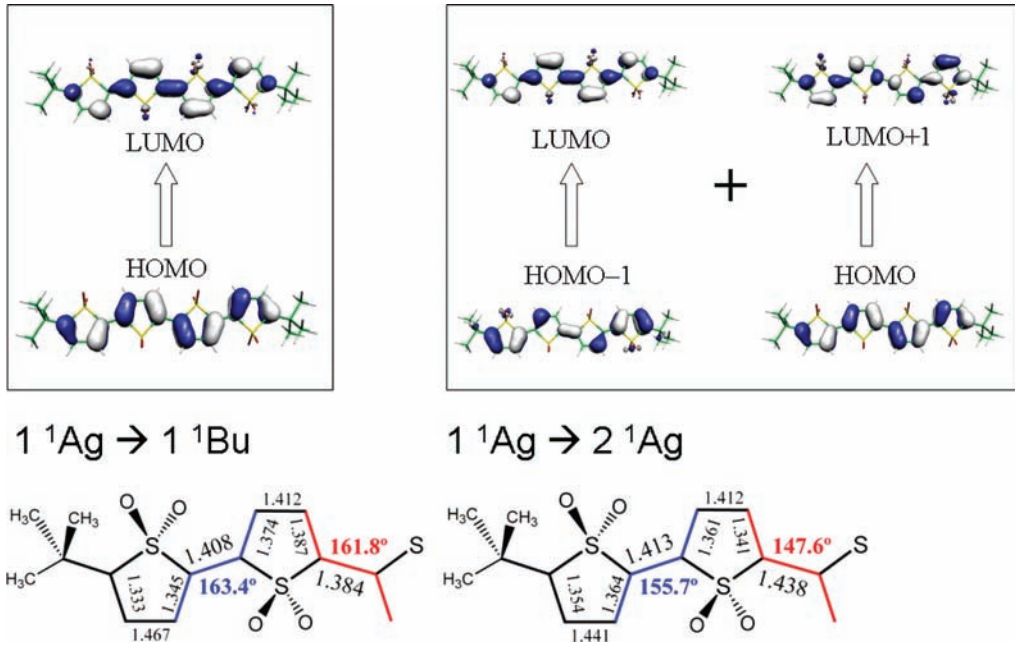

Figure 4. (Top) Orbital involved in the relevant excitations predicted by TD-DFT//B3LYP/6-31G** in **4TSO** and their topologies. (Bottom) RCIS/HF/3-21G* optimized geometries of both states (S_1 and S_2) are represented.

electronic state and first excited state in **EDO4T** rather than due to the planarity imparted by the S···O inter-ring interactions. By comparing the theoretical changes of the central C−C bond on transitioning from S_0 to S_1 (Figure 4 and Figure S2, Supporting Information), it is observed that for **4TSO** the central C−C bond shortens by 0.054 Å, while for **4T** the decrease is larger (0.070 Å). This would indicate that the vibrational frequencies in S_1, regarding those of S_0, would be more different in **4T** than in **4TSO** also originating some portion of the spectral broadening on the absorption spectrum of **4T** compared to its dioxide analogue.

2.2. Photophysical Properties and Nature of the Low-Lying Excited States. 2.2.1. Excited-States Ordering: A Theoretical Insight. Although the experimental absorption spectra cannot be used to explain the $S_0 \rightarrow S_2$ transition because of the forbidden character of the $1^1A_g \rightarrow 2^1A_g$ excitation for the C_{2h} symmetry in **4T** and **4TSO** (i.e., considered as planar), the evolution of this transition, as explored with TD-DFT, is summarized in Table 1. This forbidden transition is always calculated as being above the $1^1A_g \rightarrow 1^1B_u$ transition.

The order of the first singlet excited states in short thiophene oligomers is very different from that observed in oligoenes with the same number of π-electrons. For instance in **T2** (the unsubstituted bithiophene), the 2^1A_g state has been located 0.8 eV above the 1^1B_u state, whereas in octatetraene (the oligoene homologue) the 2^1A_g state is 0.6 eV lower than the 1^1B_u state.[8c,14,15] Moreover, when the chain length of the oligothiophene is increased, the energy of the dipole-forbidden 2^1A_g state decreases to a greater extent than that of the dipole-allowed (1^1B_u) one.[16,17,18c] This brief description of the excited-state order in oligothiophenes and oligoenes is central to our ongoing analysis since it describes the basic properties that dioxide oligothiophenes might show under the hypothesis that these are in between the former two. The optimized structures for the $1^1A_g \rightarrow 1^1B_u$ and $1^1A_g \rightarrow 2^1A_g$ excitations together with the orbitals description are displayed in Figure 4. A $1^1B_u/2^1A_g$ energy reversal is established on passing from oligothiophenes to oligoenes; the first excited singlet is generally found to be the 1^1B_u state in oligothiophenes; however, the fact that double excitations (HOMO,HOMO→LUMO,LUMO), which are contained in the $1^1A_g \rightarrow 2^1A_g$ configuration, are very sensitive to electron−electron correlation overall leads to a greater stabilization of the $1^1A_g \rightarrow 2^1A_g$ single excitation in molecules with a large number of correlated π-electrons such as oligoenes.[15−19]

The evaluation of the relative position of the $1^1B_u/2^1A_g$ states is required for a proper analysis of the photophysical properties of our materials, with a caveat that the effects of correlation and the contribution of double excitations must be properly estimated.[15−19] Multiple active space multiconfigurational self-consistent field wave functions (ORMAS MCSCF) with second-

(14) Birnbaum, D.; Kohler, B. E. *J. Chem. Phys.* **1989**, *90*, 3506.
(15) (a) Zerbetto, F.; Zgierski, M. Z. *J. Chem. Phys.* **1988**, *89*, 3681. (b) Negri, F.; Orlandi, G.; Zerbetto, F.; Zgierski, M. Z. *J. Chem. Phys.* **1989**, *91*, 6215. (c) D'Amico, K. L.; Manos, C.; Christensen, R. L. *J. Am. Chem. Soc.* **1980**, *102*, 1777. (d) Tavan, P.; Schulten, K. *J. Chem. Phys.* **1986**, *85*, 6602. (e) Brédas, J. L.; Heeger, A. J. *Chem. Phys. Lett.* **1989**, *154*, 56. (f) Pierce, B. M. *J. Chem. Phys.* **1989**, *91*, 791. (g) Soos, Z. G.; Ramasesha, S. *Phys. Rev. B* **1984**, *29*, 5410.
(16) (a) Birnbaum, D.; Kohler, B. E. *J. Chem. Phys.* **1992**, *96*, 2492. (b) Beljonne, D.; Shuai, Z.; Brédas, J. L. *J. Chem. Phys.* **1993**, *98*, 8819.
(17) (a) Rubio, M.; Merchán, M.; Pou-Amérigo, R.; Ortí, E. *ChemPhysChem* **2003**, *4*, 1308. (b) Rubio, M.; Merchán, M.; Ortí, E.; Roos, B. O. *J. Chem. Phys.* **1995**, *102*, 3580. (c) Rubio, M.; Merchán, M.; Ortí, E. *ChemPhysChem* **2005**, *6*, 1357. (d) Rubio, M.; Merchán, M.; Ortí, E.; Roos, B. O. *Chem. Phys. Lett.* **1996**, *248*, 321.
(18) (a) Grebner, D.; Helbig, M.; Rentsch, S. *J. Phys. Chem.* **1995**, *99*, 16991. (b) Seixas de Melo, J.; Silva, L. M.; Kuroda, M. *J. Chem. Phys.* **2001**, *115*, 5625. (c) Becker, R. S.; Seixas de Melo, J.; Maçanita, A. L.; Elisei, F. *J. Phys. Chem.* **1996**, *100*, 18683. (d) Burrows, H. D.; Seixas de Melo, J.; Serpa, C.; Arnaut, L. G.; Hamblett, I.; Navaratnam, S. *J. Chem. Phys.* **2001**, *115*, 9601. (e) Raganato, M. F.; Vitale, V.; Della Sala, F.; Anni, M.; Cingolani, R.; Gigli, G.; Favaretto, L.; Barbarella, G.; Weimer, M.; Görling, A. *J. Chem. Phys.* **2004**, *121*, 3784. (f) Ginochetti, G.; Galiazzo, G.; Mazzucato, U.; Spalletti, A. *Photochem. Photobiol. Sci.* **2005**, *4*, 547. (g) Paa, W.; Yang, J. P.; Rentsch, S. *Appl. Phys. B: Laser Opt.* **2000**, *71*, 443.
(19) Della Sala, F.; Heinze, H. H.; Görling, A. *Chem. Phys. Lett.* **2001**, *339*, 343.

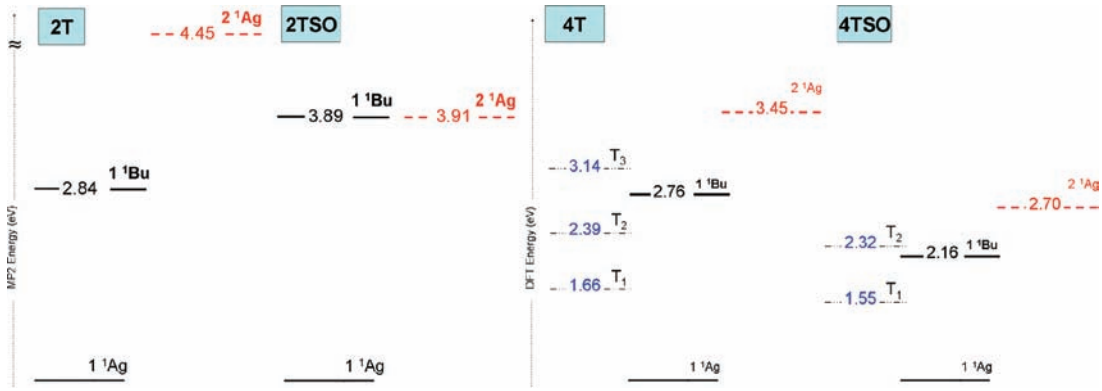

Figure 5. Energy diagram showing: (Left) MCQDPT2 distribution of the singlet excited-state energies in **2T** and **2TSO**. (Right) Singlet and triplet manifolds according to TD-DFT calculations in **4TSO** (left) and in **4T** (right).

order quasi-degenerate multiconfigurational perturbation theory (MCQDPT2) corrections for the state energies have been carried out for **2T** and **2TSO** in order to estimate the incidence of sulfonation in the excited states (Figure 5). In **2T** the first excitation $1A_g \rightarrow 1B_u$ ($S_0 \rightarrow S_1$) is calculated at 2.84 eV followed by the $1A_g \rightarrow 2A_g$ (i.e., $S_0 \rightarrow S_2$) at 4.45 eV. In contrast, the second dipole-forbidden excitation of **2TSO** is greatly stabilized relative to the dipole-allowed one; $1A_g \rightarrow 1B_u$ and $1A_g \rightarrow 2A_g$ are calculated at 3.89 and 3.91 eV, respectively, at the MCQDPT2 level with an active space of 16 orbitals. With increasing orbital correlation, 19 orbitals of active space, the $1A_g \rightarrow 1B_u$ is almost unaltered at 3.91 eV and the $1A_g \rightarrow 2A_g$ is decreased at 3.66 eV at the MCQDPT2 level (see Supporting Information for a more exhaustive comparison). Unlike in the **2T** molecule, where the S_1 was an isolated $\pi-\pi^*$ $1B_u$ state, **2TSO** is found to have nearly degenerate S_1 and S_2 states. At the highest correlation treatment level used here, the $2A_g$ state appears to be the S_1. However, since it is separated from the dipole-allowed $1B_u$ S_2 by only 0.25 eV, the ordering of the two states may be changed with further improvements in the basis set and correlation treatment. Both the S_1 and S_2 excitations in **2TSO** originate from an electron transfer from the sulfoxide p-orbitals to the carbon π-system, with the only difference being the phase of the contributions due to the neighboring sulfoxide units (see Figure S3, Supporting Information). As a result, these excitations should remain close in energy. Similar observations may be expected to apply to longer oligomers of *S*,*S*-dioxide thiophenes. This MCQDPT2 excited-state description will have a critical influence in the photophysics of the *S*,*S*′-dioxide oligothiophenes, such as it will be attempted to demonstrate next.

2.2.2. Emission Spectra: Oligoene-like Vision. The emission spectra of the compounds in this study are displayed in Figure 6. The first observation is that the fluorescence quantum yield decreases on going from the oligothiophenes to their dioxide derivatives. Despite the low quantum efficiency of *S*,*S*′-dioxide oligothiophenes, the emission spectra of **2TSO** and **3TSO** were successfully recorded at room temperature in dichloromethane. Typical vibronic features associated with the planarization of the S_1 state are displayed in the fluorescence emission spectra of **2T** (Figure 6) and **3T** (Figure S4, Supporting Information), while the Stokes shift values are found to be in consonance with the ground state to be composed by several conformers. Contrasting observations are found in **2TSO** and **3TSO**, as the luminescence spectra are observed to be featureless and significantly red-shifted.

As already mentioned, a decrease of the fluorescence emission upon going from the oligothiophenes to their dioxides counterparts is observed with a further decrease on increasing the chain length. Moreover it is interesting to note that in contrast with the oligothiophenes, where fluorescence and intersystem crossing (ISC) were the main deactivation pathways for S_1 with a negligible internal conversion (IC),[18c] the *S*,*S*′-dioxide oligothiophenes fluorescence and ISC are basically absent and 99% (Table 2 and S2) of the quanta are lost through IC. These findings might be in agreement with the participation of the dipole-forbidden nonemissive 2^1A_g (2^1A_1) state close to the emissive 1^1B_u (1^1B_1) in molecules with C_{2h} (C_{2v}) molecular symmetry such as predicted in previous section as revealed by the MCQDPT2 data.

There are, however, more data supporting these statements. The excitation and emission spectra of **2TSO** in toluene are displayed in Figure 7 where the following details are observed: (i) the absorption spectrum due to the $1^1A_g \rightarrow 1^1B_u$ is clearly reproduced in the excitation spectrum, obtained at the maximum

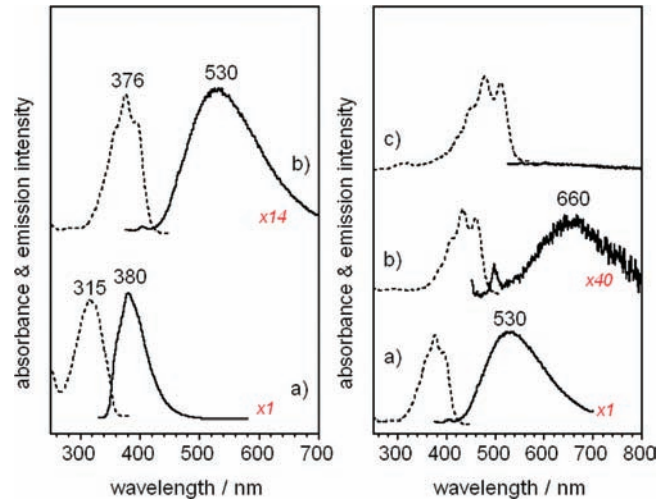

Figure 6. (Left) Absorption and emission spectra of (a) **2T** and (b) **2TSO** at 25 °C in dichloromethane. (Right) Absorption and emission spectra of (a) **2TSO**, (b) **3TSO**, and (c) **4TSO** at 25 °C in dichloromethane.

Table 2. Fluorescence Quantum Yields, Fluorescence Lifetimes, and Radiative (k_F) and Nonradiative (k_{NR}) Rate Constants of **2TSO** in THF, Toluene, and Decaline

	Φ_F	τ_F [ns]	$k_F{}^a$ [ns^{-1}]	$k_{NR}{}^b$ [ns^{-1}]
THF	0.004	0.58	0.0069	1.72
toluene	0.007	0.92	0.0076	1.08
decaline	0.012	1.61	0.0075	0.61

^{a} $k_F = (\phi_F)/(\tau_F)$. ^{b} $k_{NR} = (1 - \phi_F)/(\tau_F)$.

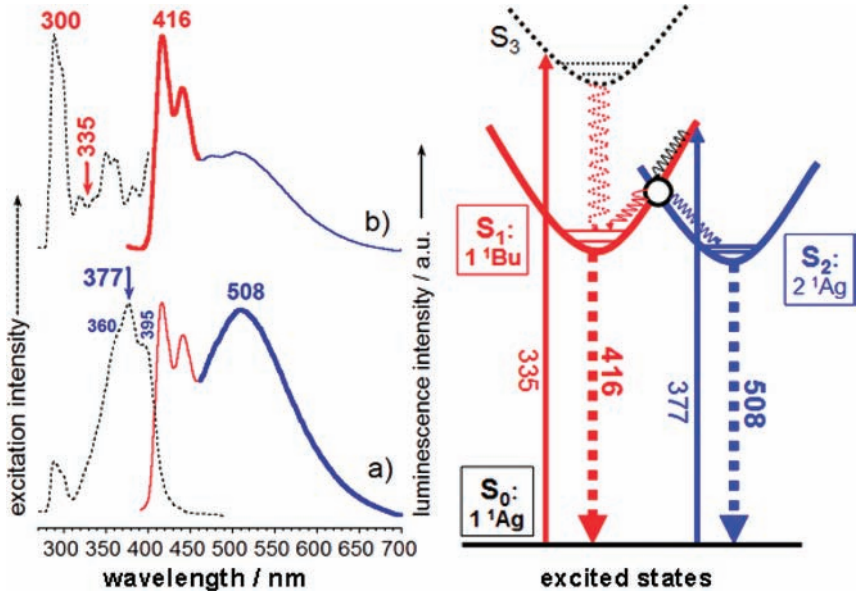

Figure 7. Left: (a) excitation (collecting at 508 nm) and emission spectra (exciting at 377 nm) of **2TSO** in toluene at room temperature. (b) Excitation (collecting at 416 nm) and emission spectra (exciting at 300 nm) of **2TSO** in toluene at room temperature. Right: Potential energy surfaces compatible with the experimental data where the white circle denotes the crossing point between the $1^1A_g/1^1B_u$ states.

of the emission band (508 nm); (ii) however, the emission peak at 416 nm provides a excitation spectrum with a maximum around 300 nm and a medium-low intensity signal in the 360−390 nm range. In Figure 7, a possible energy surface disposition that could account for the experimental peaks under the assumption of interaction of the dipole-allowed and -forbidden singlet states is depicted. To better understand this steady-state photoluminescence, one additional factor concerning oligoenes (i.e., carotenoids) must be considered since the 1^1B_u to 2^1A_g crossing between the two low-lying excited states mostly takes place upon exclusive excitation of the S_1 (1^1B_u), while by exciting electronic states at higher energy, followed by internal conversion to the S_1 (1^1B_u), the crossing to the 2^1A_g is partially hindered.[20] This would explain that the excitation spectrum of the $2^1A_g \rightarrow 1^1A_g$ emission is the $1^1A_g \rightarrow 1^1B_u$ absorption, while the $1^1B_u \rightarrow 1^1A_g$ emission is mostly produced by excitation at higher energies (from 300 to 360 nm). In any case, for **2TSO** both 416/508 nm emissions are observed upon excitation either the S_1 or the S_n states though the relative intensity pattern certainly follows the above indications. Nonetheless, it must be highlighted that the detection of absorption and the emission from this 2^1A_g is the consequence of the underlined state mixing. Partial fluorescence quenching in **2TSO** and in **3TSO** and full disappearance of emission in **4TSO** is observed due to the stronger state coupling and subsequent increase in electron correlation present in the longer *S*,*S*′-dioxide oligomers.

The large red-shifts of the maxima of the emissions from **2TSO** to **3TSO**, and consequently large Stokes shifts as well, are also in agreement with these coming from the potential energy surface minima of the 2^1A_g state placed below the electronic origin of the strongly absorbing state. Another interesting observation, corroborating our hypothesis, concerns the broad and featureless aspect of the observed emissions that correlates with the more distorted geometry predicted for the $1^1A_g \rightarrow 2^1A_g$ excitation compared to the $1^1A_g \rightarrow 1^1B_u$ one such as seen in Figure 4. This increasing movement or easiness of rotation around the central dihedral angle in the minimum of the 2^1A_g state on excitation would impart a larger flexibility resulting in spectral broadening.

2.2.3. Solvent Dependence of the Emission Properties. Similar to that observed in oligoenes,[17] the excited-state interaction is strongly dependent on the environment, and a solvent dependence of the emission properties is thus expected. The works of Barbarella et al. on the photophysical properties of *S*,*S*-dioxide oligothiophenes should be considered as a reference in this field.[4] In recent contributions,[21] it is concluded that the emission efficiency is controlled by the S_1-S_0 internal conversion as experimentally deduced by measuring these efficiencies in solvents of different polarity and viscosity. In order to check these effects on the emission properties of our all *S*,*S*-dioxide derivatives, the fluorescence spectra in toluene and decaline are compared in Figure 8 (see Table S1, Supporting Information, for the viscosity of the solvents); the fluorescence quantum yield is observed to increase on going to the most viscous decaline, in agreement with Barbarella work, due to the decreasing efficiency of the interfering IC processes (lifetimes and kinetic constants for the radiative and nonradiative channels are presented in Table 2).

However, the profile of the emission spectrum in decaline is similar to that in dichlorometane and rather different to that in toluene. In the two former cases, radiative emission goes from the 2^1A_g singlet (i.e., at lower energy) whereas in toluene emission proceeds from the two 1^1B_u and 2^1A_g singlets. We have obtained for **2TSO** the optimized geometries at the HF/3-21G* of the three relevant electronic states: for the S_0 the interthiophene distortion is around 157.1°, for S_1 or 1^1B_u is distorted by 167.1° while for the S_2 it amounts to 146.4°. In any case the required conformational movement around this dihedral angle from the ground electronic state conformation

(20) Walla, P. J.; Linden, P. A.; Hsu, C. P.; Scholes, G. D.; Fleming, G. R. *Proc. Natl. Acad. Sci. U.S.A.* **2000**, *97*, 10808. Pang, Y.; Jones, G. A.; Prantil, M. A.; Fleming, G. R. *J. Am. Chem. Soc.* **2010**, *132*, 2264.

(21) Anni, M.; Della Sala, F.; Raganato, M. F.; Fabiano, E.; Lattante, S.; Cingolani, R.; Gigli, G.; Barbarella, G.; Favaretto, L.; Görling, A. *J. Phys. Chem. B* **2005**, *109*, 6004.

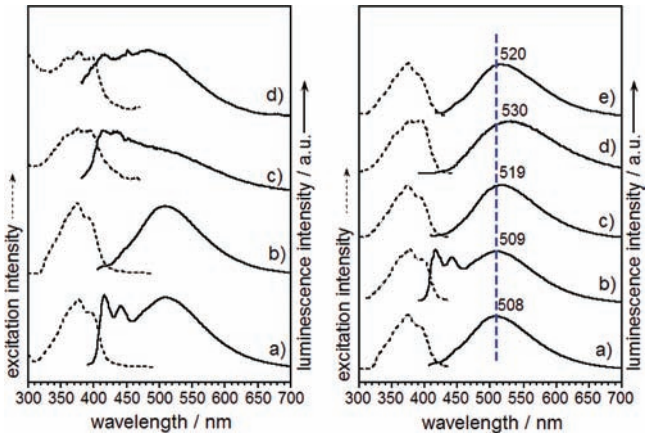

Figure 8. Left: (a) Excitation and emission spectra of **2TSO** in toluene at room temperature, (b) excitation and emission spectra of **2TSO** in decaline at room temperature, (c) excitation and emission spectra of **2TSO** in butyronitrile at room temperature, and (d) excitation and emission spectra of **2TSO** in butyronitrile at 77 K. Right: emission spectra of 2TSO in (a) decaline, (b) toluene, (c) THF, (d) dichloromethane, and (e) ethanol.

(i.e., adiabatic state) might be favored to the 2^1A_g state since its more distorted geometry (i.e., entropic-like behavior). Such as observed in Figure 8, the lowest-lying $2^1A_g \rightarrow 1^1A_g$ emission displays certain dependence of the emission maxima with the solvent polarity showing a red-shift with increasing solvent polarity. The 22 nm red-shift from decaline to dichlorometane would mean that this state could have some charge transfer character owing to the introduction of the dioxide electron polarizable groups. Interestingly, the conformational effect in decaline, on one hand, and the charge transfer stabilization in dichloromethane on the other would, in different ways, favor the emissions from the same 2^1A_g state such as observed in the spectra.

2.2.4. Temperature Dependence of the Emission Properties. To obtain additional insights on these phenomena, the emission spectra of **2TSO** in butyronitrile at room and low temperatures (77 K, Figure 8) have been collected. In all cases, prior to photon emission, a thermal equilibration is found to exist between the intervening excited states. With only one active excited state, little dependence on the emission profile with temperature is commonly expected. However, in our case and given the similar energy of the $1^1B_u/2^1A_g$ states, the thermal equilibrium between these two states is governed by a rather small energy difference [i.e., $\Delta E(E_{1^1B_u} - E_{2^1A_g})$] possibly on the order of k_BT; consequently, the thermalization in this case might be temperature-dependent. At 77 K, it is observed in the emission that the band with the maximum around 500−510 nm is strengthened relative to the same fluorescence band at room temperature. A similar explanation to that presented in the previous section can account for the emission from the 2^1A_g lower-energy state. Upon cooling, a more vitreous (viscous) or rigid matrix, such as decaline, is expected with the same effect as for the more active emission state. Also, the strengthening on cooling of the charge transfer interactions with butyronitrile might be another plausible reason favoring the emission from the CT 2^1A_g state.

2.2.5. Emission Spectra: Oligothiophene-like Vision. In the preceding sections, the photophysical properties of the dioxide oligothiophenes have been addressed from the point of view of oligoene-like properties. A similar analysis from the perspective of the optical properties of oligothiophenes is attempted now. In thienyl oligomers, two main deactivation channels are well established. The first channel, intersystem crossing (ISC) to the triplet state manifold, is thought to be particularly important in thiophenes due to the heavy-atom effect of sulfur. The second deactivation channel, $S_1 \rightarrow S_0$ internal conversion, is considered particularly effective in the case of low band-gap systems as a result of the energy-gap law.[21]

Table 3. Two-Photon Absorption Cross Sections (δ in GM units) Measured by the Two-Photon Excitation Fluorescence at 820 nm in Dichloromethane of the Six Studied Compounds

2T	0.017	**2TSO**	1.0
3T	2.2	**3TSO**	10.5
4T	30.1	**4TSO**	40.1

In Figure 5, the second vertical triplet state (i.e., T_2) of **4TSO** is situated within 0.16 eV of S_1, while for **4T** this singlet−triplet energy gap is larger (0.38 eV). It is deduced that according to the energy-gap law $S_1 \rightarrow T_n$ intersystem crossing would be more efficient in the case of the dioxide oligothiophenes which is an additional factor explaining their low fluorescence efficiency. Moreover, this singlet−triplet energy gap is concomitantly reduced on **2TSO→4TSO** also in agreement with the decrease of the radiative properties on increasing chain length. In order to find an experimental proof of this ISC, two additional experiments have been carried out: (i) low-temperature emission spectra have been recorded, with no additional bands from $T_1 \rightarrow S_0$ phosphorescence detected; and (ii) flash-photolysis in polar ethanol has been done for **3T** and **3TSO**. For the former, given in Figure S6 (Supporting Information), the appearance of a band around 470 nm, compatible with $T_1 \rightarrow T_n$ transitions among triplet states, is observed in transient spectra after microsecond timing. Surprisingly, for **3TSO**, no transient spectra are detected in these experimental conditions, an observation which can be rationalized in terms of a faster quenching of these triplet excitons (see Table S2, Supporting Information). Moreover, the likely, very low value of ϕ_{ISC} (in any case ≥ 0.01) is given by the very low singlet oxygen yield ($\phi_\Delta = 0.01$ in Table S2, Supporting Information). At this point it must be mentioned that the broad emission bands recorded for **2TSO** and **3TSO** which are extensively red-shifted relative to the absorption is a property typical of phosphorescence. Nonetheless, these emissions cannot be assigned to $T_1 \rightarrow S_0$ transitions because of the very short lifetimes (7−10 ns), and because the transitions displayed in Figure 7 were obtained at room temperature, where triplets would very likely to be quenched. In any case, direct observation of these high-spin excited states turns out to be spectroscopically elusive for these dioxide oligothiophenes, as it also happens for phosphorescence in most of oligothiophenes.[22]

2.3. Two-Photon Absorption Measurements. The presence of the dipole-forbidden 2^1A_g state in the *S,S′*-dioxide oligothiophenes has been proven indirectly by theoretical calculations, by the quenching of fluorescence and in the last section by Raman spectroscopy. However, a straight spectroscopic proof for the existence of these dark states will be provided only by two-photon absorption spectroscopy, taking advantage of the two-photon activity of the same parity $A_g \rightarrow A_g$ excitations. The two-photon absorption cross sections measured in the six samples by the two-photon excitation fluorescence technique are collected in Table 3.

Common trends are observed within the nonoxidized and oxidized samples such as the dependence of TPA cross sections

(22) Becker, R. S. *Theory and Interpretation of Fluorescence and Phosphorescence*; Wiley-Interscience:: New York, 1969.

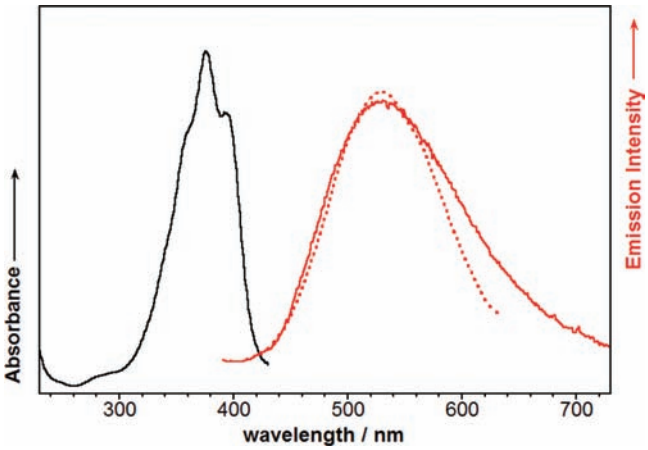

Figure 9. Absorption (black line) and one-photon (red solid line, excitation at 400 nm) and two-photon emission (red dotted line, excitation at 800 nm) of a 10^{-4} M solution of **2TSO** in CH_2Cl_2.

with conjugation length and HOMO−LUMO gaps.[23] A notable increment of the TPA activity, also increasing with conjugation length, is produced by selective oxidation of the sulfur atoms. The presence of a low-lying energy A_g TPA-active excited state, or $1A_g \rightarrow 2A_g$ transition, is straightforwardly related to the TPACS evolution from oligothiophenes to their respective sulfones; with the same 800 nm excitation, the sulfone derivatives are found to be considerably more active as two-photon absorbers as a result of the shift of this state to lower energies. In the case of **2TSO**, the one-photon and two-photon emission spectra are depicted in Figure 9 with perfect overlap, indicating that both emissions depart from the same minimum energy point, corresponding to the $2A_g$ excited state.

It can be argued that the **4T→4TSO** δ increment presented above is simply due to the HOMO−LUMO reduction resulting from oxidation (see section 2.1). However, the relative increment is much more modest than expected upon a quite significant HOMO−LUMO reduction of ∼80 nm and is thus assigned to the role played by the one-photon $2A_g$ dark state. In addition, the TPACS is found to moderately increase with the number of oligothiophene units, an effect that, together with the conjugation length increment, might also be partially explained by the energy lowering of the first A_g excited state and the increase in the accessibility of this state by 820 nm two-photon excitation.[23]

2.4. Raman Spectra, Molecular Structure and Vibrational Properties. 2.4.1. Raman Spectra and π-Conjugation. As shown in Figure S7 (Supporting Information), the experimental 1064 nm FT-Raman spectrum of **4TSO** is accurately predicted by the DFT//B3LYP/6-31G** theoretical Raman, in which the line at 1527 cm^{-1} is given by the symmetric C═C stretching modes of the terminal rings, whereas the lines at 1480 cm^{-1} are caused by the symmetric C═C stretching on the central rings (see normal modes in Figure S8, Supporting Information).[24] Stronger Raman-active normal modes are found in the center rather than in the molecular periphery as a result of the relative ease of

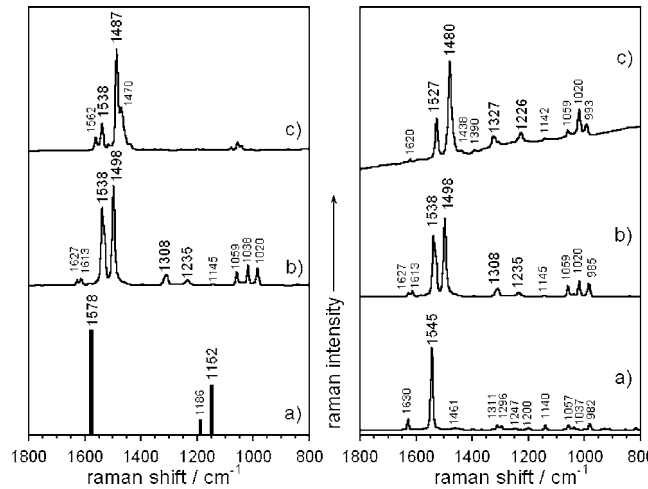

Figure 10. Left: Solid-state Raman spectra of: (a) **3OE** represented as bars keeping the experimental relative intensities as in ref 12; (b) **3TSO**, and (c) **3T**. Right: (a) **2TSO**, (b) **3TSO**, and (c) **4TSO**.

polarization of the central site and the subsequent larger contribution to the molecular polarizability.

From the assignment above, it must be emphasized that none of these vibrational modes directly involves the sulfur atoms or the connected oxygen atoms; however, their selective oxidation in **3T**, for example, provokes the alteration of its Raman spectral frequencies and intensities in Figure 10, in agreement with the indirect **3T→3TSO** perturbation of the π-conjugational path resulting from the removal of thiophene aromaticity of the sulfur p_z electrons.

In particular, oxidation displaces the C═C stretches to higher frequencies; for example, the strongest line at 1487 cm^{-1} in **3T** is blue-shifted by 11 cm^{-1} in **3TSO**, in line with the 0.02−0.03 Å strengthening of the C═C bonds after sulfonation according to the theoretical ground electronic state S_0 geometries in Figure 11. These strong Raman lines are directly associated with the effectiveness of π-electron conjugation along the C═C/C−C backbone sequence and is the reason by which these lines were used in section 2.1.1 (Figure 3) for the discussion of the molecular conformers.

The two characteristic Raman lines of polyacetylene[12] are observed in the spectrum of di(terbutyl) *all-trans*-12-hexaene (**3OE**, as bars in Figure 10) with one Raman-active ν(C═C) mode at 1578 cm^{-1} and the ν(C−C) mode at 1152 cm^{-1}.

Within the dioxide series there is a progressive red-shift of the ν(C═C) frequencies with the increment of chain units: this is readily observed in the behavior of the strongest Raman line, 1545 cm^{-1} in **2TSO**, 1498 cm^{-1} in **3TSO**, and 1480 cm^{-1} in **4TSO**. This tendency has been related in many oligothiophenes and oligoenes series to the extension of π-electron conjugation along the skeletal backbone in the ground electronic state as a consequence of the increasing number of available π-electrons.[24] However, this effect is also seen in the S_0 geometries; for example, the innermost C═C distances are elongated: 1.353 Å in **2TSO**, 1.358 Å in **3TSO**, and 1.360 Å in **4TSO**, in agreement with the relaxation of the double bond and the subsequent decrease of the vibrational stretching energy.

2.4.2. Raman Spectra and Electronic States. Determining the signatures of the competition of the $1^1A_g \rightarrow 2^1A_g$ and $1^1A_g \rightarrow 1^1B_u$ excitations, critical for the photophysics of these molecules, is accomplished by scanning the vibrational Raman spectra. To this end, assessment of the Raman excitation spectroscopy is

(23) Thienpont, H.; Rikken, G. L. J. A.; Meijer, E. W.; ten Hoeve, W.; Wynberg, H. *Phys. Rev. Lett.* **1990**, *65*, 2141. Periasamy, N.; Danieli, R.; Ruani, G.; Zamboni, R.; Taliani, C. *Phys. Rev. Lett.* **1992**, *68*, 919.

(24) (a) Casado, J.; Katz, H. E.; Hernandez, V.; Lopez Navarrete, J. T. *J. Phys. Chem. B* **2002**, *106*, 2488. (b) Hernández, V.; Casado, J.; Ram, F. J.; Zotti, G.; Hotta, S.; Lopez Navarrete, J. T. *J. Chem. Phys.* **1996**, *104*, 9271.

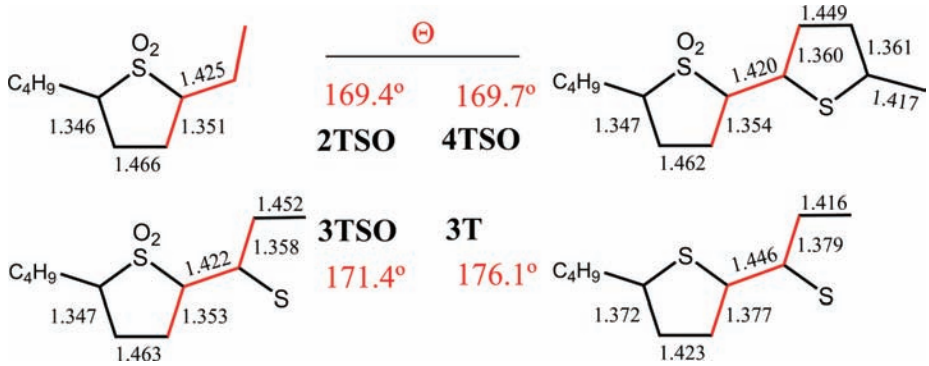

Figure 11. Ground electronic state DFT//B3LYP/6-31G** optimized geometries of some of the studied compounds.

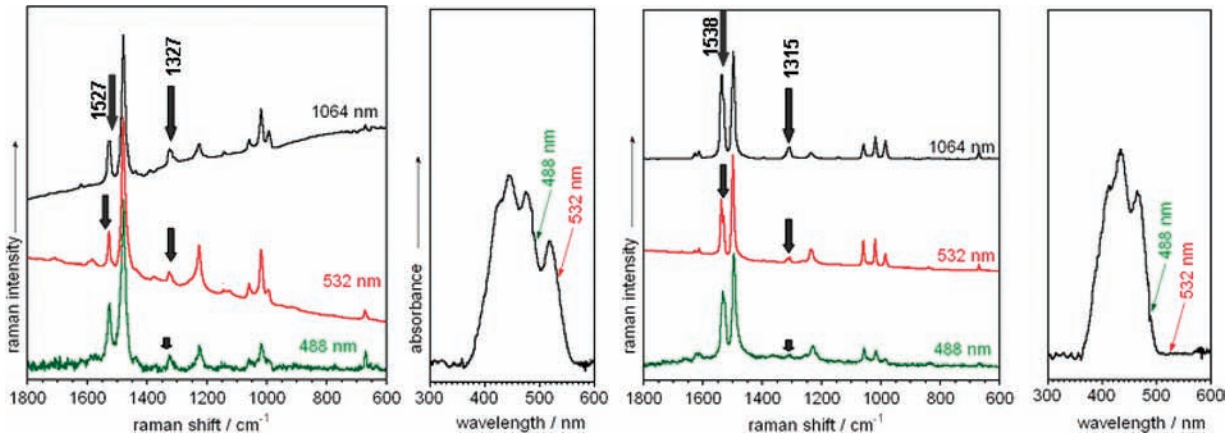

Figure 12. Left: Solid-state Raman and UV−vis spectra of **4TSO** recorded with three excitation wavelengths. Right: The same for **3TSO**. Raman spectra are normalized to the strongest Raman line.

accomplished in order to make visible the 2^1A_g state by the intervention of the selection rules of the Raman experiment by means of a proper tuning of the laser-Raman excitation wavelength.[25]

An adaptation of this method will be used here in which, instead of a nanometer-to-nanometer tuning of the laser-Raman wavelength, three or four laser wavelengths encompassing a large interval of the excitation spectrum are used. Therefore, in what follows, the Raman spectra as a function of the excitation wavelength are inspected with the purpose of distinguishing the contribution of the interacting excited electronic states. It is hypothesized that by exciting with shorter-wavelength lasers (i.e., 532 and 488 nm) a resonance mainly with the $1^1A_g \rightarrow 1^1B_u$ electronic absorption (Figure 12) will be obtained, whereas by pumping with the 1064 nm laser, the sum-overstates polarizability term will be covered with contributions primarily from the low-lying dipole−dipole-forbidden $1^1A_g \rightarrow 2^1A_g$ excitation. As such, this transition may be rendered active by the selection rules for the two-photon vibrational Raman process. This can be also understood by the incorporation of the Herzberg−Teller term in the formula of the Raman intensity[26] where dipole-forbidden electronic states may be coupled through a relevant vibrational mode. By means of comparisons between these short and long excitation wavelength spectra, information of the excited states of interest can be assessed.

A clear resonance with the dipole-allowed $1^1A_g \rightarrow 1^1B_u$ excitation, manifested in the 0−0 and 0−1 vibronic peaks centered at 518 and 475 nm, respectively, in the solid-state spectra, is obtained in the Raman spectra of **4TSO** taken with the 532 and 488 nm laser lines. A similar situation is found in the **3TSO** spectra, in which the 488 nm spectrum is observed to be in resonance with the 0−0 vibronic peak. The three following properties are observed: (i) the lines at 1327 and 1315 cm^{-1} in **4TSO** and **3TSO** are weakened on passing from the nonresonant 1064 nm spectrum to the in-resonance 488 nm (488 and 532 nm for **4TSO**) spectra. These weak bands in the Raman spectrum correspond to the strongest infrared bands as deduced by assigning the IR spectrum of **4TSO** according to its DFT/B3LYP/6-31G** theoretical spectrum (Figures S9 and S10, Supporting Information), and they can be described as the stretching modes of the S−O bonds. (ii) The weakening of the 1520−1550 cm^{-1} ν(C═C) mode of the terminal rings is another feature assessed by comparing the in- and nonresonance spectra. The third property, (iii), is concerned with the more complex aspect of the 1064 nm spectrum as compared to the spectra obtained through resonant excitation. In case (i), if it is assumed that the primary spectral contribution is due to the $1^1A_g \rightarrow 2^1A_g$ excitation, the signatures of the HOMO−1 and LUMO+1 are expected to appear according to the TD-DFT assignment. Relative to the HOMO and LUMO, the orbitals below and above are expected to have large involvement of the oxygen atoms of the S−O bonds (see Figure 4), so that the intensity weakening of the ν(S−O) band in the spectrum resonating with the HOMO→LUMO excitation ($1^1A_g \rightarrow 1^1B_u$) is well addressed. The greatest geometrical changes affecting the C═C bonds are taking place in the outermost rings for the $1^1A_g \rightarrow 2^1A_g$ excitation, the 1064 nm Raman spectrum covering it, would show some

(25) Thrash, R. J.; Fang, H. L. B.; Leroi, G. E. *J. Chem. Phys.* **1977**, *67*, 5930.
(26) Albrecht, C. A. *J. Chem. Phys.* **1961**, *34*, 1476.

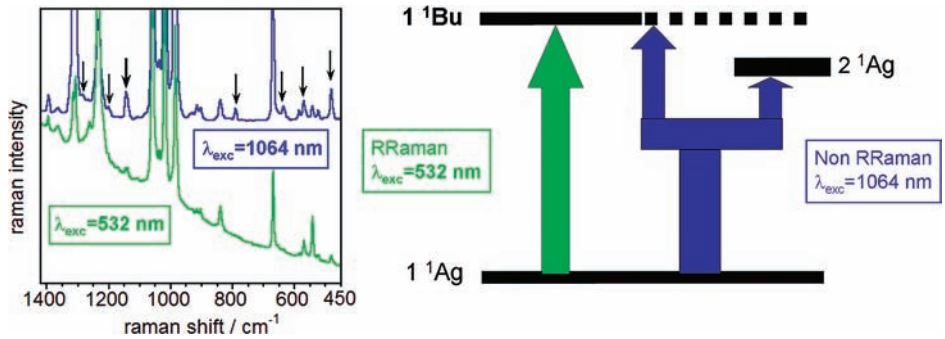

Figure 13. Left: 1064 nm (blue) and 532 nm (green) enlarged Raman profiles of **3TSO** with arrows denoting the new, or enhanced, bands in the two-level covered Raman spectrum. Right: Coupling of the relevant electronic excited states in the Raman process as a function of the excitation Raman energy (RRaman denotes resonance Raman conditions).

enhancement coming from the C=C vibrational modes at the molecular periphery, which is also a consequence of the largest electron densities on these rings in the HOMO−1 and LUMO+1 orbitals. Finally, case (iii) can be similarly explained since the spectral simplification associated with the resonance Raman process which only enhances the chromophore vibrational bands involved in the corresponding excitation. This is readily observed in the enlarged Raman profiles displayed in Figure 13.

Under the hypothesis that the 1064 nm wavelength would excite two electronic transitions, one would expect a larger number of Raman-active vibrations. In other words, the resonance case is accounted for exclusively by the pure electronic term or vibronic A term of the Albrecht Raman intensity formula, while in the nonresonance case, the B term or the Herzberg−Teller portion of the formula together with the A term accounts for the total Raman intensity distribution among the molecular vibrational modes. A scheme (Figure 13) is proposed to visualize the phenomenon considered for explaining the vibrational band profile of the Raman spectra.

3. Final Discussion and Conclusions

Directly related with our compounds there are two close contributions in the literature. First is a recent example of sulfur *S,S′*-dioxides (fluorene-dibenzothiophene-*S,S′*-dioxides)[27] having a donor−acceptor−donor substitution pattern. Here the authors show that these oligomers exhibit dual fluorescence due to the presence of two competing excited states, a local excited state and a highly twisted intramolecular charge transfer excited state, or TICT state. Second, and with reference to oligoenes, it is well-known that carotenoids[20,28] and short oligoenes exhibit dual fluorescence owing to the interaction/coupling of close-lying B_u/A_g energy states, the same argument that we have explained and explored here. It has been our hypothesis that dual emission in our samples arises from their oligoene character, which is not in contradiction with the explanation in the fluorene-dibenzothiophene dioxides since: (i) it has been theoretically predicted that this $1^1A_g \rightarrow 2^1A_g$ excitation possesses an intramolecular charge transfer character (i.e., from the π-conjugated path to the dioxide groups in our oligothiophene dioxides); and (ii) it has been described that the $2^1A_g \rightarrow 1^1A_g$ emission features a moderate dependence with the solvent polarity ascribable to its CT character. In contrast, the 1^1B_u state mostly involves the carbon skeleton and by this reason has more Frenkel exciton character (tentative precursor of a local exciton state). As a consequence, both existing fluorene-dibenzothiophene-*S,S′*-dioxide and carotene (short oligoene) visions result in a common situation which anticipates the existence of this dual photoluminescent effect in our oligothiophene dioxides. Aside from these dioxide examples, there are intriguing cases of quenching of fluorescence in some conjugated molecules (the reasons for which are not fully known yet), for example, the family of oligothiophenevinylene oligomers, with a mixture of thiophene and vinylene groups that could certainly represent a new case of $1^1B_u/2^1A_g$ excited-state interference at the origin of the fluorescence quenching.

The elucidation of the photophysical mechanisms involved in light emission are critical for the rational design of new electroluminescent and/or photovoltaic materials; in the former case, optimizing dual emission wavelength can lead to the achievement of a broader spectrum of lighting, whereas for light harvesting, the excited-state energy sequence is critical for efficient energy transfer among the multichromophoric components in the photon-to-charge conversion effect. In summary, the optical and photophysical properties of a series of *S,S′*-dioxide oligothiophenes together with their structural features in the ground and relevant excited electronic states have been addressed by using a combination of spectroscopic and theoretical techniques. Their emission properties are featured by a strong quenching of fluorescence imparted by the interaction of an A_g (A_1) excited state [i.e., possible ICT state] close in energy to that of the absorbing B_u (B_2) [i.e., possible local exciton state]. We have been able to find out that dual fluorescence comes from these two low-lying excited states and to provide spectroscopic proofs of their presence (i.e., strong solvatochromic and thermal dependent emissions, Raman and two-photon absorption) together with a complete and exhaustive theoretical description of the electronic structure based on DFT and high level ab initio methods. The same has been done for the structural properties on the basis of the Raman spectra which shows a scenario of absence of thiophene aromaticity since removal of the π (p_z)-electrons of the sulfur which thus renders diene-like character to the five-member ring. Overall we see that the strategy of full sulfonation of oligothiophenes might represent an interesting organic synthetic protocol with benefits in (i) red-shifting of the optical properties, (ii) improving the electron-accepting redox capability, and (iii) promoting a broadening of the emission profile.

(27) Dias, F. B.; Pollock, S.; Hedley, G.; Palsson, L. O.; Monkman, A. P.; Perepichka, I. I.; Perepichka, I. F.; Tavasli, M.; Bryce, M. R. *J. Phys. Chem. B* **2006**, *110*, 19329. King, S. M.; Perepichka, I. I.; Perepichka, I. F.; Dias, F. B.; Bryce, M. R. *Adv. Funct. Mater.* **2009**, *19*, 586.

(28) Bettermann, H.; Bienioschek, M.; Ippendorf, H.; Martin, H. D. *Angew. Chem., Int. Ed.* **1992**, *31*, 1042.

Another interesting topic highlighted in this paper is the rationalization that functionalization at the sulfur atom of the thiophene (i.e., oxidation), little explored in the field, might be a versatile way to attain new materials with new optical properties for semiconducting and luminescent substrates which are prospects of interest for the scientific community working in organic electronics.

Acknowledgment. The present work was supported in part by the Dirección General de Enseñanza Superior (DGES, MEC, Spain) through research project CTQ2009-10098. We are also indebted to Junta de Andalucía for the project FQM4708/2009. J.C. is grateful to the MEC of Spain for I3 professorship. M.M.O is indebted to the MEC for a predoctoral fellowship. J.S.d.M. acknowledges financial support from the Portuguese Science Foundation (FCT) through FEDER and POCI. M.R.H. acknowledges financial support from the NGA.

Supporting Information Available: Additional spectroscopic, photophysical, and computational details. This material is available free of charge via the Internet at http://pubs.acs.org.

JA101015Q